

## Chain Stiffness of Donor–Acceptor Conjugated Polymers in Solution

Scott P. O. Danielsen, Colin R. Bridges, and Rachel A. Segalman\*



Cite This: *Macromolecules* 2022, 55, 437–449



Read Online

ACCESS |



Metrics & More

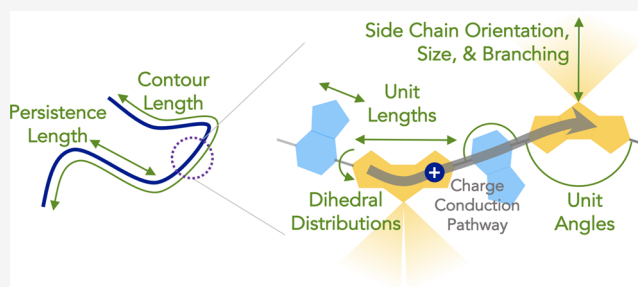


Article Recommendations



Supporting Information

**ABSTRACT:** The optoelectronic properties of conjugated polymers are dictated by their chain conformations, which depend on the interplay of delocalization of electrons along the  $\pi$ -conjugated backbone and the intrachain interactions of pendant side chains. Here, we leverage small-angle neutron scattering to measure the chain shapes of several classes of commonly used, high mobility donor–acceptor conjugated polymers in dilute solution. We find that these model conjugated polymers are semiflexible with persistence lengths ranging from several to hundreds of nanometers, dependent on the molecular structure of the polymer, indicating the importance of repeat unit geometry, particularly side-chain size and branching, on the overall chain conformations. The measured persistence lengths show good agreement with those calculated according to dihedral distributions predicted from density functional theory. Larger persistence lengths are shown to correlate with increased charge-carrier mobility, signifying the importance of rational molecular design to obtain high persistence length organic semiconductors and thus advantageous optoelectronic properties.



### INTRODUCTION

Conjugated polymers have considerable potential for the low-cost and high-throughput production of lightweight, flexible, and large-area optical and electronic devices because of their mechanical robustness and solution processability. Solution-processable conjugated polymers are the result of substantial structural engineering:  $\pi$ -conjugated backbones that determine the optoelectronic properties and peripheral solubilizing side chains. Many promising high-performance organic semiconductors follow a donor–acceptor (D–A) motif, in which a repeat unit consists of alternating electron-rich and electron-deficient units, setting up a local electron density gradient along the backbone.<sup>1</sup> These polymers have received significant attention due to their distinctive optoelectronic properties, including small band gaps, high charge-carrier mobilities, and broad light-absorption ranges. Copolymers composed of building blocks based on diketopyrrolopyrrole (DPP), cyclopentadithiophene (CPDT), indacenodithiophene (IDT), benzothiadiazole (BT), fluorobenzothiadiazole (FBT), pyridalithiadiazole (PT), thiophene (T), and others have been explored (Figure 1).<sup>2–4</sup> Interestingly, many of these materials display high charge-carrier mobilities ( $>10 \text{ cm}^2 \text{ V}^{-1} \text{ s}^{-1}$ ) despite poor long-range structural order through quasi-one-dimensional transport along the backbone and occasional intermolecular hopping through short  $\pi$ -stacking chain contacts.<sup>5–9</sup>

The desirable properties of D–A copolymers are believed to stem from the low energetic disorder conferred by a uniform distribution of nearly planar, largely torsion-free conformations of the conjugated backbone.<sup>10,11</sup> Intramolecular charge trans-

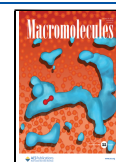
port along the conjugated polymer chain is controlled by the relative dihedral angles of monomer units along the conjugated backbone. When adjacent units are coplanar, the overlap of  $\pi$ -orbitals is maximized and the transport of electrons (or holes) is efficient.<sup>12</sup> Significant torsion, however, reduces the  $\pi$ -orbital overlap, creating conformational traps that localize charge carriers. Intermolecular charge transport is also maximized by significant  $\pi$ -orbital overlap, primarily through  $\pi$ – $\pi$  stacking and local chain contacts.<sup>13–17</sup> Thus, the key to designing high-performance conjugated polymers is permitting more efficient intra- and intermolecular charge transport at the segmental level,<sup>8,9,18</sup> spurring intense interest in identification of structure–property relationships.<sup>10,11</sup>

The chain stiffness is quantified by the persistence length  $l_p$ , which is the characteristic length scale of the exponential decay of backbone tangent–tangent correlations. The ratio of the persistence length  $l_p$  to the contour length  $L_c$  determines the statistical behavior of the chain conformations. If  $l_p \ll L_c$  then the chain behaves like a flexible coil and can be described by a random walk of Kuhn segments of length  $b = 2l_p$ ; conversely, when  $l_p \gg L_c$  the polymer behaves like a rigid rod. In the intermediate, semiflexible regime,  $l_p \approx L_c$  polymers are well described as wormlike chains. The intrinsic persistence lengths

**Received:** October 26, 2021

**Revised:** December 14, 2021

**Published:** January 5, 2022



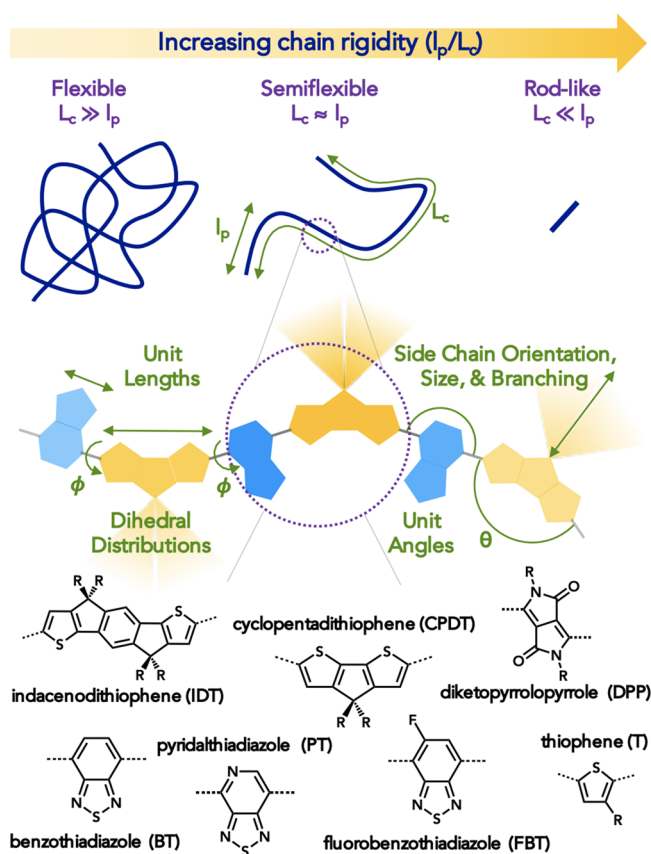


**Figure 1.** Chain statistics are governed by the ratio of the persistence length  $l_p$  to the chain contour length  $L_c$ . Conjugated polymers are often experimentally in the intermediate semiflexible regime, with their behavior crucially dependent on their persistence length, which depends critically on unit lengths, angles, and dihedral distributions between monomers and side-chain orientation, size, and degree of branching. Adapted with permission from ref 23.

and accessible chain lengths of conjugated polymer chains typically result in semiflexibility—appearing to be rigid at length scales smaller than their persistence length and flexible at larger length scales.<sup>19</sup> The persistence lengths of conjugated polymers vary widely from a nanometer to hundreds of nanometers due to their complex molecular architecture: depending strongly on varying degrees of electron delocalization, steric interactions between side chains, and geometric factors such as the bond and dihedral angles between monomers (Figure 1).<sup>20–22</sup>

While earlier work by us and others on the chain shape of organic semiconductors focused on homopolymers, primarily polythiophenes,<sup>21,23–28</sup> polyfluorenes,<sup>29</sup> and poly(*p*-phenylenevinyls),<sup>30,31</sup> the connection between the molecular structures of D–A conjugated polymers and their chain shape is receiving increased attention.<sup>15,16,32–34</sup> The chain conformations and persistence lengths of polythiophenes, in particular, have been extensively studied as a function of regioregularity, solvent, and side chain to reveal (surprisingly) flexible polymers with persistence lengths of  $\approx 30$  Å.<sup>21,23–28</sup> The inherent flexibility of polythiophenes arises from significant backbone torsion around two coplanar states, termed the *syn* and *anti* conformations. While both coplanar conformations preserve  $\pi$ -conjugation, the *syn* conformation curves the backbone, resulting in a loss of chain persistence.<sup>21</sup> This is opposite to many other common conjugated polymers, where the conjugation lengths are typically shorter than the persistence length. Thus, there is a need to investigate the chain shape of conjugated polymers containing more complex, heterogeneous molecular structures and understand the impact of this mesoscopic length scale on optoelectronic properties.

In this work, we systematically investigate the chain rigidity of donor–acceptor conjugated polymers in dilute solution. Persistence lengths, measured by small-angle neutron scattering (SANS), of a range of conjugated polymers show good agreement with persistence lengths calculated according to dihedral distributions from density functional theory (DFT). Side-chain size and branching, in particular, are shown to

**Table 1.** Molecular Characteristics, Including Calculated ( $l_p^{\text{DFT}}$ ) and Measured ( $l_p^{\text{SANS}}$ ) Persistence Lengths, for a Range of Conjugated Polymers Used in This Study

polymer	solvent	$M_n$ (g mol <sup>-1</sup> )	$\mathcal{D}$	$N$	$l_0$ (Å)	$l_p^{\text{DFT}}$ (Å)	$l_p^{\text{SANS}}$ (Å)
PCPDPT-nC16	C <sub>6</sub> D <sub>3</sub> Cl	23000	2.0	30	12.0	44.9	61.0
PCPDPT-HD	C <sub>6</sub> D <sub>3</sub> Cl	22900	1.3	30	12.0	44.9	47.3
PCPDPT-ODD	C <sub>6</sub> D <sub>3</sub> Cl	26200	1.8	30	12.0	44.9	54.9
PCPDPT-ene-HD	C <sub>6</sub> D <sub>3</sub> Cl	22900	2.0	30	12.0	48.0	76.6
PCPDPT-ene-ODD	C <sub>6</sub> D <sub>3</sub> Cl	26800	1.8	30	12.0	48.0	83.4
PCPDTFBT-C1-BO	C <sub>6</sub> D <sub>3</sub> Cl	19000	1.7	14	23.5	71.1	67.0
PCPDTFBT-C3-BO	C <sub>6</sub> D <sub>3</sub> Cl	23000	1.9	16	23.5	71.1	78.4
PCPDTFBT-C4-BO	C <sub>6</sub> D <sub>3</sub> Cl	22000	1.8	15	23.5	71.1	86.4
PCPDTFBT-C5-BO	C <sub>6</sub> D <sub>3</sub> Cl	29000	2.1	19	23.5	71.1	114
PCPDTFBT-C11-BO	C <sub>6</sub> D <sub>3</sub> Cl	101000	1.9	53	23.5	71.1	291
PIDTFBT-C11-BO	C <sub>6</sub> D <sub>3</sub> Cl	24000	2.0	7	32.2	(>1 μm) <sup>a</sup>	(254) <sup>b</sup>
PIDTBT-nC16	C <sub>6</sub> D <sub>3</sub> Cl	64500	2.3	50	16.0	(>1 μm) <sup>a</sup>	(1310) <sup>c</sup>
PIDTBT-nC16	CDCl <sub>3</sub>	64500	2.3	50	16.0	(>1 μm) <sup>a</sup>	(1340) <sup>c</sup>
PIDTCPDT-C11-BO	C <sub>6</sub> D <sub>3</sub> Cl	14000	1.3	6	19.8	224	(236) <sup>b</sup>
PDPPTPyT-ODD	C <sub>6</sub> D <sub>3</sub> Cl	62000	1.6	61	20.9	78.4	84.6

<sup>a</sup>Persistence length predicted by the DFT hindered-rotating chain method indicates rigid-rod behavior. The actual persistence length would be sensitive to bond bending, chain defects, etc. <sup>b</sup>Persistence length obtained by the wormlike chain model fit to the SANS data is comparable to the contour length, indicating that the result might be chain length sensitive, and a higher molecular weight polymer would be necessary for resolution. <sup>c</sup>Persistence length obtained by the wormlike chain model fit to the SANS data is outside the measured  $q$  range. Scattering at smaller angles would be necessary for resolution.

introduce substantial changes in the persistence lengths of conjugated polymers containing the same aromatic conjugated backbone. These results indicate the importance of structural engineering in determining the chain shape of conjugated polymers and elucidate molecular design strategies for development of new high performing D–A copolymers.

## MATERIALS AND METHODS

**Materials and Molecular Characterization.** Deuterated solvents were obtained from Cambridge Isotope Laboratories. All other solvents and reagents were purchased from Fisher Scientific and Sigma-Aldrich. Solvents were dried, degassed, and stored over molecular sieves under a nitrogen atmosphere prior to use. Milli-Q ultrapure water (18.2 M $\Omega$  cm at 25 °C) was used in all synthetic procedures.

Monomers and other precursors were synthesized according to the literature procedures.<sup>35–39</sup> Cyclopentadithiophene-*co*-pyridalithiadiazole (PCPDTP), cyclopentadithiophene-*co*-fluorobenzothiadiazole (PCPDTFBT), indacenodithiophene-*co*-benzothiadiazole (PIDTBT), and indacenodithiophene-*co*-fluorobenzothiadiazole (PIDTFBT) polymers were prepared via a palladium-catalyzed Stille cross-coupling polymerization in a xylenes/dimethylformamide mixed solvent under microwave irradiation (Biotage Initiator Eight Microwave System, 200 W, 2.45 MHz), precipitated into methanol, filtered, washed with methanol and ethyl acetate, Soxhlet extracted into hexanes, purified on a silica gel column with chloroform as the eluent, and finally concentrated in vacuo to obtain green-blue solids.<sup>35–37,39</sup> Indacenodithiophene-*co*-cyclopentadithiophene (PIDTCPDT) polymers were prepared in a nitrogen glovebox via a palladium-catalyzed Stille cross-coupling polymerization at 110 °C in xylenes, precipitated into methanol, filtered, washed with methanol and ethyl acetate, Soxhlet extracted into chloroform, purified on a silica gel column with chloroform as the eluent, and finally concentrated in vacuo to obtain a purple solid.<sup>39</sup> Diketopyrrolopyrrole-*co*-pyridine-*co*-thiophene (PDPPPpT) polymers were prepared in a nitrogen glovebox via a palladium-catalyzed Stille cross-coupling polymerization at 130 °C in chlorobenzene, precipitated into methanol, filtered, washed with methanol and hexanes, Soxhlet extracted into chloroform, purified on a silica gel column with chloroform as the eluent, and finally concentrated in vacuo to obtain a purple solid.<sup>38</sup>

Size-exclusion chromatography was performed using a Waters system (Waters Alliance HPLC 2695) with two Agilent PolyPore 5  $\mu$ m columns. Chloroform with 0.25% triethylamine at 25 °C was used as the mobile phase with a flow rate of 1 mL/min. A refractive index detector (Wyatt Optilab rEX), photodiode array detector (Waters 2996 PDA), viscometer (Wyatt ViscoStar), and low-angle light scattering detector (Wyatt DAWN HELEOS II, 663.1 nm laser) were used to access the absolute molecular weight and molecular-weight distribution of the polymers.<sup>40</sup> The number-average molecular weight  $M_n$  and dispersity  $\mathcal{D}$  are reported in Table 1. Full dissolution and the absence of large aggregates were confirmed by dynamic light scattering with a DynaPro NanoStar using a laser power of 100 mW and a wavelength of 662 nm.

**Small-Angle Neutron Scattering.** Small-angle neutron scattering (SANS) of polymers in dilute solution yields ensemble-averaged molecular information regarding the chain conformation (i.e., form factor) with high resolution over multiple length scales.<sup>41</sup> The scattering contrast in SANS for polymer solutions originates from the difference in the scattering cross section between the deuterated solvent and the hydrogenous polymer chains.

Scattering studies were conducted on the 30 m SANS instrument (NGB-30) at the National Institute of Standards and Technology Center for Neutron Research (NCNR)<sup>42</sup> and the extended Q-range small-angle neutron scattering diffractometer (EQ-SANS BL-6) line at the Spallation Neutron Source (SNS) located at Oak Ridge National Laboratory (ORNL).<sup>43</sup> Polymers were dissolved in deuterated solvent at a concentration of 2 mg/mL to minimize contribution to the SANS signal from interchain correlations and suppress aggregation. Vortexing, sonication, and mild heating (up to 35 °C) were used to

aid in complete dissolution. Solutions were placed into sample cells with quartz windows and 2 mm path length.

SANS measurements on NGB-30<sup>42</sup> (NCNR) used three sample–detector distances (1.3, 4, and 13 m) with a neutron beam wavelength,  $\lambda$ , of 6 Å yielding a  $q$  range of 0.004–0.4 Å<sup>-1</sup>, where the scattering variable is  $q = (4\pi/\lambda) \sin(\theta/2)$  and  $\theta$  is the scattering angle. All scattering patterns were azimuthally symmetric and reduced to a circularly averaged intensity,  $I(q)$ . Empty cell, blocked beam, transmission, background, and sample thickness corrections were made, and the averaged data were placed on an absolute cross-sectional scale. Data reduction followed standard procedures implemented in NCNR SANS packages for Igor Pro.<sup>44</sup> The incoherent scattering was estimated from the high- $q$  scattering intensity and was subtracted prior to model fitting to yield the coherent scattering intensity  $I_{\text{coh}}(q)$ .

SANS measurements on EQ-SANS<sup>43</sup> (SNS, ORNL) used a sample–detector distance of 4 m and was operated in a 60 Hz frame-skipping mode with a minimum wavelength,  $\lambda$ , setting of 2.5 Å, providing two wavelength bands (2.5–6.1 and 9.4–13.4 Å). The measured intensity was corrected for detector sensitivity and the scattering contribution from the solvent and empty cells, azimuthally averaged, and placed on an absolute scale by using a calibrated standard.<sup>45</sup> Data reduction followed standard procedures implemented in Mantid.<sup>46,47</sup>

The measured scattering profiles indicate that the studied conjugated polymers are semiflexible chains, as expected due to their large persistence lengths and relatively small degrees of polymerization (Table 1). To obtain quantitative conformational information, the wormlike chain model which describes a chain of contour length,  $L_c$ , as a sequence of locally stiff segments of persistence length,  $l_p$ , is used to model the scattering from the semiflexible polymers (full derivation in the Supporting Information).<sup>48,49</sup> At high molecular weights ( $L_c \gg l_p$ ), the wormlike chain description can be mapped to a freely jointed chain model with Kuhn length,  $b = 2l_p$ .

Except for the most rigid chains, the scattering profiles of the studied conjugated polymers exhibit a plateau at low  $q$ , indicative of the Guinier regime for random coils (i.e., at length scales smaller than or comparable to the chain size). The IDT-BT copolymer, PIDTBT–nC16, however, maintains an  $I \sim q^{-1}$  scaling even at the lowest wave vectors, indicating rigid-rod behavior at length scales accessible to SANS and thus persistence lengths >1000 Å. Several samples additionally exhibit an upturn in scattering at low  $q$  beyond the Guinier plateau as is commonly observed in conjugated polymers even in the absence of aggregation.<sup>21</sup> The cause of this low- $q$  scattering is unclear but must be due to large length scale correlations, possibly long-range electronic coupling from the  $\pi$ -conjugated backbones.

**Density Functional Theory.** Here, we will compare the persistence lengths extracted from the SANS scattering curves to the theoretical predictions calculated following an approach by Milner et al.<sup>20</sup> Dihedral potentials were computed via density functional theory (DFT) calculations using Spartan 18 with the  $\omega$ B97X-D long-range exchange correlation functional<sup>50</sup> and a 6-31G\*(d,p) diffuse, polarized, split-valence double- $\zeta$  basis set. Although limiting,<sup>51,52</sup> for computational efficiency, the torsional potentials  $U(\phi)$  were calculated by using optimized scans of the central dihedral angle(s)  $\phi$  of a repeat unit (rather than longer oligomers), and the side chains were replaced with methyl groups.

Computed torsional potential energy surfaces are shown in Figures S1–S7, with dihedral angles relative to the *anti* configuration, as shown by the chemical structures labeled in the figure insets. All studied comonomer rotamers exhibit an absolute energy minimum for the *anti* configuration (centered at  $\phi = 0^\circ$ ) and a relative energy minimum for the *syn* configuration (centered at  $\phi = 180^\circ$ ), but with differing degrees of the steepness of the torsional potential and thermally accessible dihedral angles. Thus, even though the isomeric energy differences are typically only several  $k_B T$  (Figures S1–S7), torsional disorder is a key determinant of the observed chain shape,<sup>20</sup>

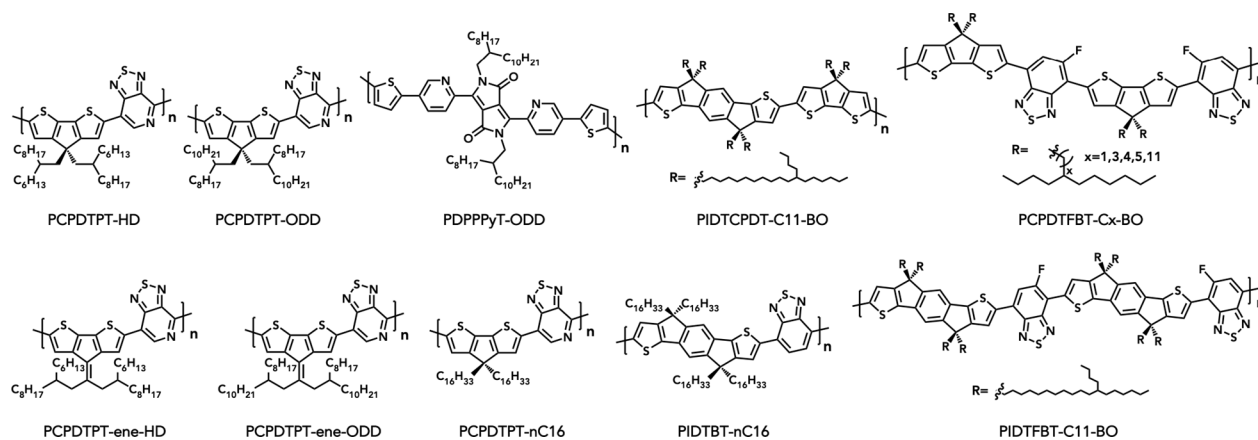


**Figure 2.** Molecular structures of conjugated polymers used in this study.

and the DFT calculations can be used to elucidate how the donor and acceptor groups affect backbone planarity.

Theoretical persistence lengths  $l_p^{\text{DFT}}$  were estimated by numerically averaging the backbone conformations over a set of suitably generated dihedral angles according to an established procedure.<sup>20</sup> Briefly, the dihedral probability distribution  $p(\phi)$  is computed by using Boltzmann factors from the dihedral potentials  $U(\phi)$ . The polymer backbone tangent–tangent correlation function  $\langle \mathbf{v}_0 \cdot \mathbf{v}_n \rangle$ , where  $\mathbf{v}_0$  and  $\mathbf{v}_n$  represent the orientations of the backbone tangent vector of monomer 0 and monomer  $n$ , is stochastically integrated according to  $p(\phi)$  over many single-chain conformations. The persistence length is extracted as a characteristic exponential decay of  $\langle \mathbf{v}_0 \cdot \mathbf{v}_n \rangle$  as

$$\langle \mathbf{v}_0 \cdot \mathbf{v}_n \rangle = e^{-nl_0/l_p} \quad (n = 0, 1, \dots, N - 1) \quad (1)$$

where  $N$  is the number of repeat units along the polymer backbone and  $l_0$  is the projected length of a repeat unit. Calculated polymer backbone tangent–tangent correlation functions for each polymer type are shown in Figures S1–S7.

## RESULTS AND DISCUSSION

The optoelectronic and mechanical properties of conjugated polymers are intimately related to their local molecular arrangement and packing, with small variations in the chain conformation leading to substantial effects on the macroscopic properties.<sup>53</sup> In general, there are several key modifications that can be made to the structure of conjugated polymers in solution: (1) modification of the  $\pi$ -conjugated backbone unit lengths through extension of the fused aromatic rings or the introduction of flexible conjugation breaking spacers, (2) alteration of and interactions between the donor and acceptor comonomers to reduce torsional disorder along their linkage, (3) variation of the pendant side chains in alkyl chain length, branching, and inclusion of ionic or other functional groups, and (4) replacement of the  $sp^3$ -bridging carbon to heavier atoms or  $sp^2$ -hybridized nitrogen or methylene units to rotate the orientation of the side chains. Many of these modifications result in changes in the chain shape and are shown in Figure 1.

Understanding of the single-chain properties, including conformations in solution, require an accurate description of the influence of these molecular structural factors, which can be partly achieved by surveying a range of D–A conjugated polymers (Figure 2) to independently tune each parameter.<sup>26</sup> Molecular characteristics, including calculated ( $l_p^{\text{DFT}}$ ) and measured ( $l_p^{\text{SANS}}$ ) persistence lengths, for a range of conjugated polymers used in this study are summarized in Table 1. Values in parentheses have uncertainty resulting from the sample or the technique and merit validation in future studies to confirm

that the results are size-invariant.<sup>54</sup> Moreover, while it is well-known that synthetic defects and differences in regioregularity can significantly decrease observed chain rigidity,<sup>21</sup> the remarkable agreement between DFT-calculated and SANS-measured persistence lengths signifies that those issues do not appreciably affect the studied materials. In fact, most of the persistence lengths measured by SANS are *higher*, in some cases significantly, than those calculated by using torsional potentials from DFT, suggesting additional factors impacting the chain shape beyond those included in the theoretical model, namely the importance of the side chains.

**Backbone.** The primary contributions to the chain rigidity of conjugated polymers are the small backbone deflection angles and steep torsional potentials. The torsional potentials (and the resulting thermally accessible dihedral angles) influence the conformations much more dramatically than bending or stretching of individual bonds.<sup>55</sup> Conjugated polymers thus typically do not achieve extremely large persistence lengths comparable to DNA ( $\sim 500$  Å) because there are two rotamers that preserve planarity (i.e., *cis/trans*), and electron delocalization tolerates a significant amount of torsion ( $\sim 30^\circ$ ) without disruption.<sup>21,56</sup>

Here, the SANS scattering data show good agreement with the wormlike chain model across a wide  $q$  range for several different classes of conjugated polymers in dilute solution (Figure 3), confirming the semiflexible nature of these polymers. Persistence lengths obtained from wormlike chain model fits to the SANS data are presented in Table 1. As the backbone is varied through choice of the donor and acceptor comonomers, the measured persistence length ranges from 54.9 Å for copolymers with nonzero deflection angles (PCPDTPT) to over 1000 Å for copolymers with minimal deflection or torsional disorder (PIDTBT).

PIDTBT, a donor–acceptor copolymer with the long fused aromatic heterocycle donor indenodithiophene (IDT) paired with the benzothiadiazole (BT) acceptor, is receiving extensive attention for exceptional properties attributed to its low energetic disorder.<sup>8,9,14,57</sup> The backbone is “wavy” but has been shown to be largely torsion-free, with small deviations from planarity ( $\phi \approx 5^\circ$ ),<sup>9</sup> as reproduced in Figure S1. The low deflection angles and minimal torsion results in a predicted  $l_p^{\text{DFT}} > 1$  μm and a measured  $l_p^{\text{SANS}} = 1310$  Å, substantially stiffer than other studied conjugated polymers and the freely rotating chain model (ignoring torsional potential energy) prediction of only 292 Å.<sup>22</sup> The IDT–BT linkage is most stable in the *anti* configuration with a most stable dihedral angle of close to  $10^\circ$

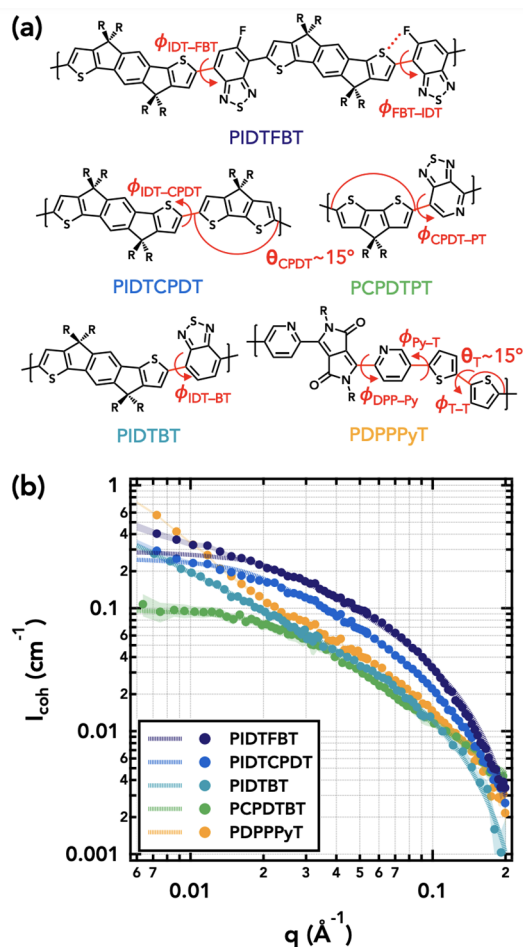


**Figure 3.** (a) Chemical structures of conjugated polymers with torsion-susceptible linkages, nonzero deflection angles, and non-covalent “lock” interactions marked in red. (b) Small-angle neutron scattering data (symbols) with wormlike chain model fits (lines) for dilute solutions ( $2 \text{ mg mL}^{-1}$  in  $\text{C}_6\text{D}_5\text{Cl}$ ) showing the effect of variation of the  $\pi$ -conjugated backbone.

and a steep torsional barrier (Figure S1). The low torsional disorder of PIDTBT has been attributed to nontraditional hydrogen bonding between the peripheral hydrogen of the IDT and the BT sulfonamide nitrogen.<sup>9</sup> Such intramolecular noncovalent “lock” interactions between adjacent units aid in increasing backbone planarity and reducing torsional disorder.<sup>13,58–60</sup>

Further modifying the acceptor unit from BT to fluorobenzothiadiazole (FBT) or pyridalithiodiazole (PT) induces stabilizing through-space  $\text{F}\cdots\text{S}$  and  $\text{N}\cdots\text{S}$  resonance interactions that provide a driving force for structure planarization, the reduction of torsional disorder, and a stronger preference for the *anti* configuration (Figures S1, S2, S5, and S7).<sup>58,61</sup> Surprisingly, however, adding a non-covalent “lock” interaction by switching the BT acceptor to FBT resulted in a lower measured persistence length for PIDTFBT of  $254 \text{ \AA}$ . It is unclear whether the reduced persistence length relative to PIDTBT is an artifact of lower molecular weight or of the steeper torsional potential (Figure S2), wherein the energetic barrier to rotation is so large that both *syn* and *anti* rotamers are statistically present but locked into their conformations during polymerization and unable to rotate. Given the intense interest in IDT-containing conjugated

polymers, the effects of the acceptor unit and noncovalent interactions<sup>62</sup> on the resultant chain shape should be further investigated.

Replacing the BT acceptor with cyclopentadithiophene (CPDT), PIDTCPDT is actually a donor–donor copolymer originally designed to produce a more rigid polymer due to the increased fused-ring content. However, because of the nonzero deflection angles of the CPDT unit, only the most stable *anti* configuration produces a linear backbone, while the *syn* configuration contributes to backbone deflections. In addition, the torsional potential of IDT–CPDT is rather soft (Figure S3), such that large deviations from the most stable rotamer are thermally accessible, leading to a distribution of dihedral angles<sup>63,64</sup> and a relatively low measured persistence length ( $l_{\text{p}}^{\text{SANS}} = 236 \text{ \AA}$ ). This agrees well with the predicted  $l_{\text{p}}^{\text{DFT}} = 224 \text{ \AA}$  from the DFT hindered-rotating chain method. It is likely that steric hindrance encourages significant non-coplanarity; the stable minima of the potential energy surface are at  $30^\circ$  and  $150^\circ$  with only a weak preference for the *anti* configuration (Figure S3).

Using CPDT as a shorter fused-ring donor copolymerized with PT, PCPDTPT, is another common D–A copolymer, but with a significantly lower persistence length ( $l_{\text{p}}^{\text{SANS}} = 54.9 \text{ \AA}$  and  $l_{\text{p}}^{\text{DFT}} = 44.9 \text{ \AA}$ ) relative to IDT-containing copolymers, again attributed to the nonzero deflection angles of the CPDT unit. Much like asymmetric fluorination of the BT unit, the asymmetry of the PT moiety strengthens an electrostatic dipole moment and interaction between the donor and acceptor, enhancing coplanarity with most stable dihedral angles of  $0^\circ$  in the *anti* configuration (Figure S5).<sup>61</sup>

Utilizing pyridine-flanked diketopyrrolopyrrole (DPP–Py) as an electron-accepting unit in connection with bithiophene, PDPPPpYt is a low-band-gap copolymer<sup>38,65</sup> with a measured persistence length of  $l_{\text{p}}^{\text{SANS}} = 84.6 \text{ \AA}$ . This is close to the predicted  $l_{\text{p}}^{\text{DFT}} = 78.4 \text{ \AA}$  and points to flexibility imparted by the deflection angles ( $\theta \sim 15^\circ$ ) and accessible dihedral angles from the thiophene linkages. T–T has a symmetric potential energy surface with minima at  $40^\circ$  and  $140^\circ$ ; T–Py is nearly symmetric, with a weak preference for the *anti* configuration and a dihedral angle of  $20^\circ$ . Py–DPP, however, is strongly asymmetric and strongly prefers a  $0^\circ$  dihedral angle locking in the *anti* configuration (Figure S4). If those flexible linkages are removed, incorporating thienothiophene (TT) instead of pyridine and thiophene, the resulting copolymer is substantially stiffer with a persistence length  $>1 \mu\text{m}$  in the near- $\Theta$  solvent  $\text{CDCl}_3$ .<sup>15</sup> This is in agreement with a study on copolymers of benzodifurandione, oligo(*p*-phenylenevinylene), and thiophene or bithiophene that showed increasing the bithiophene content (reducing thiophene content) primarily affected the unit angles, resulting in a more linear backbone conformation, increased rodlike behavior, and enhanced  $\pi$ -stacking.<sup>66</sup>

Finally, it is useful to compare the persistence lengths of the D–A conjugated polymers studied here with values from literature for other classes of conjugated polymers and correlate with optoelectronic properties. Most of the D–A copolymers have persistence lengths on par with the few existing measurements ( $50\text{--}90 \text{ \AA}$ ),<sup>22,34</sup> only a factor of 2–3 larger than poly(3-alkylthiophenes).<sup>21,27,28</sup> The (obvious) exception is for copolymers incorporating the extended fused-ring IDT, which exhibit substantial rigidity and persistence lengths 10 $\times$  or more than poly(3-alkylthiophenes).

Although the electronic properties of organic semiconductors are dependent on molecular weight as well as synthetic, processing, and device conditions, we find a general qualitative trend of increased charge-carrier mobility with increased persistence length: P3ATs  $\lesssim$  PCPDTs  $<$  PDPPyT  $<$  PIDTs.<sup>35,37,57,58,65,67</sup> This has been previously predicted, as stiff coplanar configurations enhance  $\pi$ -conjugation encouraging intramolecular charge transport.<sup>5,7,68</sup> However, it is important to note that additional processing can change the charge-carrier mobility of most materials by several orders of magnitude, in large part because the electronic properties depend on both intra- and interchain interactions (particularly crystallization) in the solid state.

While more rigid chains also tend to enhance short contacts between chains enhancing  $\pi$ - $\pi$  stacking and intermolecular charge transport,<sup>8,9,17</sup> the exact microstructure of the polymer in the active layer is critically important.<sup>6,14,18</sup> For example, a higher content of planar fused rings correlates with enhanced electrical conductivity,<sup>57,69</sup> although ring expansion alone is not sufficient to encourage coplanarity; persistence lengths and charge-carrier mobilities are decreased if the bulky aromatic rings cause steric hindrance and additional torsion elsewhere in the chain.<sup>58,70,71</sup> Additionally, a larger degree of conformational freedom (often lowering the persistence length) can actually assist the chain segments in achieving higher crystallinity, and thus higher charge-carrier mobility, as is suspected for polythiophenes.<sup>72,73</sup> It is suggestive that the optical absorption for such flexible-in-solution polymers (thiophene and CPDT-containing) changes dramatically upon solidification as the chains order, while the intrinsically higher persistence length polymers (DPP and IDT-containing) exhibit little change in their optical spectra.<sup>63,72,74–77</sup> Collectively, these results reinforce that chain rigidity of constituent conjugated polymers, as quantified by the persistence length, is one of several factors that contribute to high performance organic electronic devices.<sup>7,11</sup>

**Side Chain.** Flexible side chains are added to conjugated polymers to promote solubility in organic solvents for solution processing, but the choice of solubilizing side chain itself dramatically affects the properties of the resultant polymer. The length, bulkiness, tethering position, and chemical nature of the side chains control the molecular packing, chain dynamics, and optoelectronic properties.<sup>12,78–88</sup> Herein, we deconvolute the effects of side-chain size, orientation relative to the backbone, and branch point location on the chain stiffness of model D–A conjugated polymers.

**Alkyl Chain Size and Orientation.** In classical (saturated) polymers, increasing the length of the side chain increases the persistence length, and it has been postulated that a similar effect exists in conjugated polymers.<sup>24,26</sup> However, increasing the side-chain length also often increases the  $\pi$ - $\pi$  stacking distance, hampering intermolecular charge transport to the detriment of the electrical conductivity.<sup>83,84</sup> Here, we investigate the effect of side chains on the persistence length of D–A conjugated polymers by measuring the chain rigidity of a series of side-chain engineered PCPDTPT copolymers (Figure 4a), previously shown to form lyotropic liquid crystals that can be used to enhance transistor performance through chain alignment.<sup>35,36</sup> Steric repulsion of the side chains is manipulated via varying the size of the side chain (2-hexyldecyl (HD) or 2-octyldecyl (ODD)) and the orientation relative to the backbone. Side chains are orthogonal to the backbone for PCPDTPT-HD and PCPDTPT-ODD and parallel for

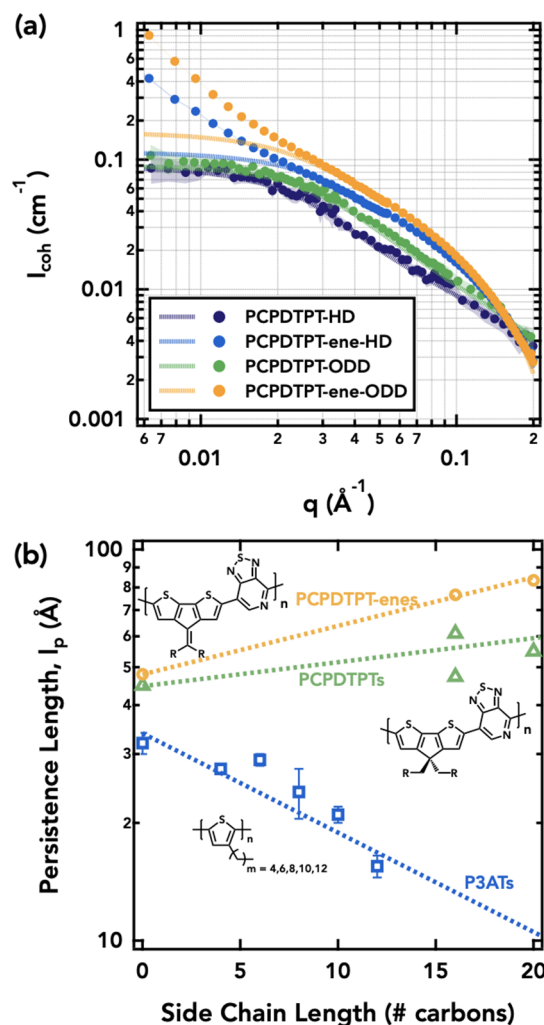


**Figure 4.** (a) Small-angle neutron scattering data (symbols) with wormlike chain model fits (lines) for dilute solutions (2 mg mL<sup>-1</sup> in C<sub>6</sub>D<sub>5</sub>Cl) of PCPDTPT conjugated polymers shown in Figure 2 showing the effect of side-chain size and rotation. (b) Persistence length as a function of side-chain length, showing opposing trends for poly(3-alkylthiophenes)<sup>21</sup> versus D–A copolymers. Reference values in the absence of side chains are predictions from the DFT hindered-rotating chain method. All other points are measured from SANS.

backbone for PCPDTPT-ene-HD and PCPDTPT-ene-ODD, which allows for closer  $\pi$ - $\pi$  stacking in the solid state.<sup>36</sup>

Increasing the side-chain size from HD to ODD modestly (10–15%) increases the measured persistence length independent of the orientation of the side chains (Figure 4b and Table 1). The persistence length increased from 47.3 Å for PCPDTPT-HD to 54.9 Å for PCPDTPT-ODD and from 76.6 Å for PCPDTPT-ene-HD to 83.4 Å for PCPDTPT-ene-ODD. Additionally, all measured persistence lengths from SANS were higher than predicted from the DFT-calculated hindered-rotating chain model, which does not consider side chains. This data shows that the persistence length increases with the size of the side chain, counter to the well-studied poly(3-alkylthiophenes), in which linear alkyl side chains of any length result in measured persistence lengths lower than the 32 Å prediction of the hindered rotating chain model using DFT-calculated torsional potentials.<sup>20</sup> In poly(3-alkylthiophenes), the persistence length decreases from 29 Å for hexyl side chains to 16 Å for dodecyl side chains (Figure 4b), attributed

to an increase in the population of *syn* conformations which have a larger accessible side-chain volume.<sup>21,82</sup> This trend has also been observed in polythiophenes with ethylene glycol side chains, where a decrease in persistence length from 61 to 31 Å was observed as the side-chain length was increased from three to four ethylene glycol units.<sup>89</sup>

These results show an increase in persistence length with side-chain size for PCPDTPT copolymers, likely due to similar accessible volume for the side chains independent of *syn* or *anti* rotation, steeper torsional potentials,<sup>20,51,90</sup> as well as low side-chain-distribution density<sup>91</sup> and side chains orthogonal to (rather than in-plane with) the backbone. Note, however, that these observed trends in persistence length are also counter to estimates from optical spectroscopy of the chain extension in lyotropic solutions where the chains with HD side chains were observed to be more extended than chains with ODD side chains.<sup>35</sup> It is possible that the seeming incongruity is due to the shorter length side chains enabling stronger  $\pi$ -stacking rather than differences in extension of isolated chains. Or, as was recently observed via contrast-variation SANS and supporting coarse-grained MD simulations, the larger side chains can result in a measured apparent persistence length of the entire chain that is substantially larger than the persistence length of just the backbone. In that study, the persistence length of poly(3-decylthiophene) was measured to be  $21.0 \pm 2.0$  Å for the entire chain but only  $10.5 \pm 1.0$  Å for the conjugated polymer backbone.<sup>28</sup>

It is thus apparent, however, that the side chains must impact the chain shape by introducing steric constraints (in solution or in the solid state) and possibly affecting the dihedral disorder of the  $\pi$ -conjugated backbone. Both CPDTP and CPDT-ene-PT linkages have asymmetric potential energy surfaces that are most stable in the *anti* configuration with a dihedral angle of 0° (Figures S5 and S6). The small torsional potential energy differences manifest in a slight increase in predicted persistence length (44.9 Å for PCPDTPTs to 48.0 Å for PCPDTPT-enes) but rather large (~50%) increases in measured persistence length, suggesting that the side chains rather than changing the hybridization of the bridging carbon are primarily responsible for the persistence length changes. For the HD side chains, rotation of the side-chain orientation increases the measured persistence length from 47.3 Å for PCPDTPT-HD to 76.6 Å for PCPDTPT-ene-HD. For the ODD side chains, rotation of the side-chain orientation increases the measured persistence length from 54.9 Å for PCPDTPT-ODD to 83.4 Å for PCPDTPT-ene-ODD. Although, it should also be noted that the PCPDTPT-ene copolymers are unattractive for optoelectronic devices due to the formation of trapped polarons on the fulvene subunit, resulting in unmeasurable charge-carrier mobilities despite closer  $\pi$ - $\pi$  stacking and more rigid chains.<sup>36</sup>

**Branch Point.** The side-chain distribution around the chain can be more simply modified by tuning the branching of the alkyl side chains. Incorporating branched rather than linear side chains has further improved the solubility in organic solvents, lowered the melting temperature, and decreased the nonradiative recombination dynamics of conjugated polymers.<sup>34–36,75,78,87,92–96</sup> The location of the branch point, relative to the conjugated backbone, has emerged as a critical parameter for controlling film morphology and device performance.

Here, measuring the chain rigidity of a series of PCPDTFBT copolymers with side chains branched at various points (Figure

5a), the persistence length is shown to dramatically increase as the branch point is moved away from the chain contour (Table

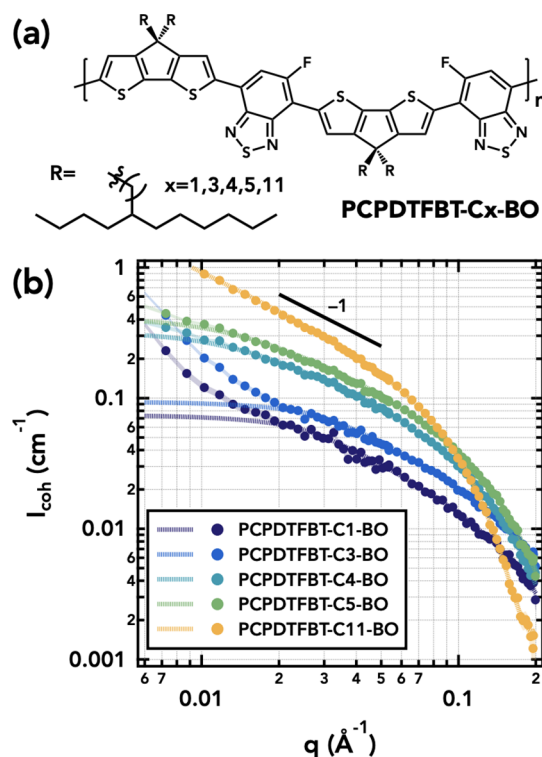


**Figure 5.** (a) Chemical structure of PCPDTFBT conjugated polymers with butyloctyl (BO) branch points at different numbers of carbons from the backbone (Cx). (b) Small-angle neutron scattering data (symbols) with wormlike chain model fits (lines) for dilute solutions ( $2 \text{ mg mL}^{-1}$  in  $\text{C}_6\text{D}_6\text{Cl}$ ) showing the strong effect of side-chain branch point location. The  $I \sim q^{-1}$  scaling indicates a rodlike scaling regime at intermediate length scales.

1 and Figure 5b). The persistence length of PCPDTFBT-C1-BO, with the butyloctyl branch only one carbon away from the backbone, has a measured persistence length of 67.0 Å, which is less than that predicted by the DFT hindered-rotating chain method ( $l_p^{\text{DFT}} = 71.1$  Å) ignoring side chains. While this is one of the rare examples in which the prediction overestimates the persistence length, side chains that are branched too close to the backbone increase steric hindrance and torsional strain, while suppressing side-chain dynamics and raising the glass transition temperature.<sup>21,80,87,97–99</sup> For instance, adding a branch point close to the backbone has been shown to decrease the conjugation and persistence lengths of poly(3-alkylthiophenes) by encouraging twisting of the chain.<sup>21,27</sup>

However, as the branch point is progressively moved farther from the backbone, the persistence length increases: 78.4 Å for three carbons away, 86.4 Å for four carbons away, 114 Å for five carbons away, and 291 Å for 11 carbons away. This correlates with enhanced coplanarity, shorter  $\pi$ - $\pi$  stacking, and higher charge-carrier mobilities as the branch point is moved away from the backbone.<sup>37,72,87,92–94</sup> In addition, qualitatively, the SANS profiles (Figure 5) show a widening range of rodlike  $I \sim q^{-1}$  scaling behavior, increased radius indicated by the approximate  $q$  value above which  $I \sim q^{-4}$  scattering is observed, and decreased uptick at low  $q$  as the branch point is moved further from the backbone. The wormlike chain model fits to the SANS data further confirm

the increase in radius of the flexible cylinder used to model the chain (Figure 6).

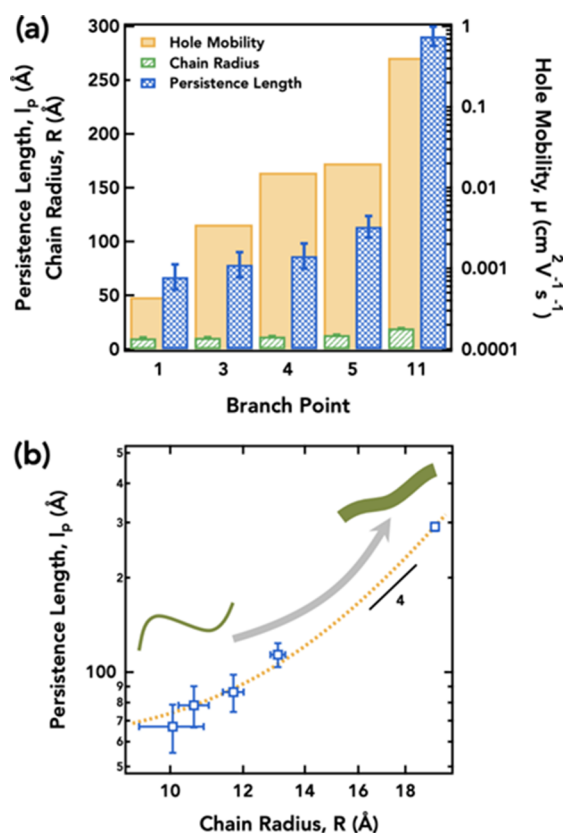


**Figure 6.** (a) Persistence length, chain radius, and reported charge-carrier mobility (ref 37) for PCPDTFBT conjugated polymers as a function of branch point location on the side chain. (b) Persistence length as a function of chain radius showing the expected  $l_p \sim R^4$  scaling, confirming the sensitivity of the chain stiffness to steric bulk in the side chains.

To understand the rigidification of the chain due to intrachain excluded volume repulsions of side chains, it is helpful to consider the chain segment as an elastic cylinder of length  $L$  and radius  $R$  with Young's modulus  $E$ . Bending this cylinder by a small angle  $\theta$  induces compression in one-half of the beam and tension in the other half. The stiffness  $S = EI$  of the beam resisting this bending deformation depends on the moment of inertia  $I$  perpendicular to the rod axis

$$I = \int_{-R}^R r^2 dr \sqrt{R^2 - r^2} = \frac{\pi}{4} R^4 \quad (2)$$

The elastic energy of this cylinder is balanced by thermal fluctuations with energy  $k_B T$  at the characteristic crossover between stiff and flexible length scales, the persistence length:

$$l_p \simeq \frac{S}{k_B T} \simeq \frac{EI}{k_B T} \propto R^4 \quad (3)$$

Thus, the persistence length should increase to the fourth power of the radius of the chain, as observed in Figure 6 by the side-chain branch-point variation in PCPDTFBT polymers. While it is challenging to explicitly design a chain with a certain radius, increasing the size and steric bulk of the side chains (or increasing the density of side-chain grafting as in bottlebrush polymers) will increase the radius and therefore the persistence

length of the chain. Furthermore, since  $l_p \sim R^4$ , the observed stiffness is extremely sensitive to minor changes in the radius of the cylinder, highlighting the importance of side-chain engineering.

It might be expected that increasing the chain radius would also increase the  $\pi$ - $\pi$  stacking distance due to the steric repulsion of the branched side chains. However, the  $\pi$ - $\pi$  stacking distance actually decreases from 3.80 to 3.55 Å as the branch point is moved from the first to the 11th carbon away from the backbone and the chain radius increases from 10.1 to 19.4 Å (Figure 7). The tighter chain packing in the solid state

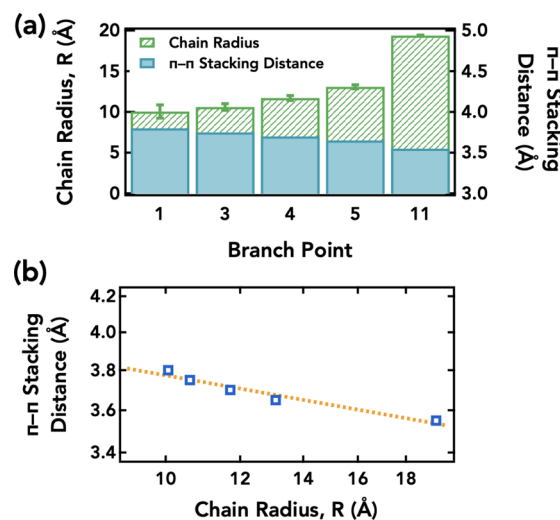


**Figure 7.** (a) Chain radius and  $\pi$ - $\pi$  stacking distance (ref 37) for PCPDTFBT conjugated polymers as a function of branch point location on the side chain. (b)  $\pi$ - $\pi$  stacking distance as a function of chain radius.

might result from enhanced nematic coupling between the stiffer chain segments. Such ordered and intimate  $\pi$ -stacking is desirable for efficient intermolecular charge transport and is likely a factor in the observed increase in charge-carrier mobility as the branch point is moved away from the chain backbone.

**Solvent.** Beyond the molecular engineering of the  $\pi$ -conjugated backbone and side chains, the choice of suspending solvent itself is a useful and tractable way to tune the conformations of conjugated polymers. Moreover, the chain shape and aggregation state in dilute solution (and intermediate structures formed during solution processing) transfer to the final solution-cast films, affecting the optoelectronic properties.<sup>35,36,100–102</sup>

The persistence lengths obtained by fitting the SANS data for PIDTBT copolymers in  $\text{C}_6\text{D}_5\text{Cl}$  and  $\text{CDCl}_3$  to the wormlike chain model are over 1000 Å with rodlike behavior across the  $q$ -range accessible by SANS (Figure 8b). Additionally, these PIDTBT copolymers are predicted by the DFT hindered-rotating chain method to be rigid rods with persistence lengths  $>1 \mu\text{m}$ ; however, it is expected that the actual persistence length should be shorter and dominated by bond bending and chemical defects. More precise experimental determination of the chain rigidity could be obtained by expanding scattering measurements to lower  $q$ .

Comparing three different classes of conjugated polymers (PIDTBT, PCPDTPT, and P3HT, Figure 2), across a wide range of chain rigidities, it is seen that the persistence lengths

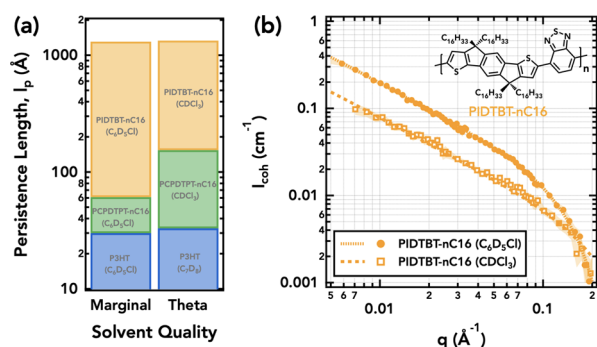


**Figure 8.** (a) Comparison of persistence lengths of conjugated polymers PIDTBT, PCPDTPT, and P3HT in marginal and  $\Theta$  solvents. The persistence length of PCPDTPT-nC16 in  $\text{CDCl}_3$  is obtained from ref 33. (b) Small-angle neutron scattering data (symbols) with wormlike chain model fits (lines) for dilute solutions ( $2 \text{ mg mL}^{-1}$  in  $\text{C}_6\text{D}_5\text{Cl}$  or  $\text{CDCl}_3$ ) of PIDTBT showing the effect of variation of the suspending solvent. The  $I \sim q^{-1}$  scaling indicates rodlike scaling even at large length scales.

are similar for polymers suspended in marginal and  $\Theta$  solvents (Figure 8a). P3HT and PIDTBT show negligible changes due to the change in solvent quality. This confirms the expectation that the local chain rigidity quantified by the persistence length should be similar between marginal and  $\Theta$  solvents, as polymers with large aspect-ratio segments weakly swell on large length scales in marginal solvents but remain  $\Theta$ -like on the scale of a persistent segment.<sup>103,104</sup> PCPDTPT, however, shows a relatively larger ( $\sim 2\times$ ) increase in persistence length changing the solvent from  $\text{C}_6\text{D}_5\text{Cl}$  to  $\text{CDCl}_3$ . This seeming discrepancy could be the result of two possibilities: (1) these measurements were not conducted on the same sample and differences could be due to molecular weight differences or other sample-to-sample variation, and (2)  $\text{CDCl}_3$  could be a poor rather than  $\Theta$  solvent with the increased  $l_p$  possibly due to solution aggregation or crystallization.

While not rigorously explored here, there has been interest recently in the solution properties of conjugated polymers in poor solvents. Solution crystallization in aromatic solvents tends to rigidify the chain, extending the measured “effective” persistence length, while the introduction of a nonsolvent decreases the measured persistence length by introducing backbone torsions as the chain collapses into globules or multichain aggregates. For example, P3HT, polyfluorene, and D–A copolymers like DPP-T-TT crystallize into nanoribbons (or nano-“whiskers”) with lengths larger than a micrometer in size, which typically further aggregate into percolating networks, “gelling” the solution.<sup>15,105–109</sup> Meanwhile, the persistence length of PCPDTPT in  $\text{CDCl}_3$  decreases from 154 Å as methanol is added and nanofibers are formed.<sup>33</sup>

## CONCLUSIONS

As organic electronics continue to advance and enter new applications, particularly those underserved by inorganic semiconductors, such as bioelectronics and flexible/stretchable devices, understanding the impact of subtle molecular changes of conjugated polymers on the chain conformations and resulting morphology and device performance will remain a fundamentally important challenge. Building upon the results discussed herein, further systematic research connecting the molecular structure to chain configurations to material

properties will continue to expand the utility and performance of these materials.

Here, we have shown that the chain shape of several classes of commonly used, high-mobility D–A conjugated polymers depends on the interplay of delocalization of electrons along the  $\pi$ -conjugated backbone and the intrachain interactions of pendant side chains. Using small-angle neutron scattering and predictions from density functional theory, we find that the chains are semiflexible, with persistence lengths ranging from several to hundreds of nanometers. Our analysis suggests several molecular design principles for creating new highly processable, low-disorder D–A conjugated polymers: (1) planar, collinear conjugated units with minimal numbers of backbone deflections or torsion-susceptible linkages per repeat unit, (2) introduction of noncovalent “locks” or other favorable interactions to generate steep torsional potentials with minima near  $0^\circ$  or  $180^\circ$ , and (3) long alkyl chains with branch points far away from the conjugated backbone to stiffen the chain and enable space-filling in the solid state without introducing backbone torsion or hindering  $\pi$ – $\pi$  close contacts. Additionally, the choice of suspending/processing solvent can be used to potentially modulate the conjugated polymer to access processability without sacrificing optimal optoelectronic performance. Thus, the heterogeneous molecular structure of donor and acceptor comonomers in D–A conjugated polymers offers nearly unlimited opportunities to tune the electronic structure, chain conformations, solution properties, solid-state morphology, and device performance through judicious molecular engineering.

## ASSOCIATED CONTENT

### Supporting Information

The Supporting Information is available free of charge at <https://pubs.acs.org/doi/10.1021/acs.macromol.1c02229>.

Details of the wormlike chain model used to fit the SANS scattering curves; dihedral potentials calculated from DFT and associated bond–bond correlation decay curves used in the calculation of theoretical persistence lengths (PDF)

## AUTHOR INFORMATION

### Corresponding Author

Rachel A. Segalman – Department of Chemical Engineering, Materials Research Laboratory, Mitsubishi Chemical Center for Advanced Materials, and Materials Department, University of California, Santa Barbara, Santa Barbara, California 93106, United States; [orcid.org/0000-0002-4292-5103](https://orcid.org/0000-0002-4292-5103); Email: [segalman@ucsb.edu](mailto:segalman@ucsb.edu)

### Authors

Scott P. O. Danielsen – Department of Chemical Engineering and Materials Research Laboratory, University of California, Santa Barbara, Santa Barbara, California 93106, United States; [orcid.org/0000-0003-3432-5578](https://orcid.org/0000-0003-3432-5578)

Colin R. Bridges – Department of Chemical Engineering, Materials Research Laboratory, and Mitsubishi Chemical Center for Advanced Materials, University of California, Santa Barbara, Santa Barbara, California 93106, United States

Complete contact information is available at: <https://pubs.acs.org/doi/10.1021/acs.macromol.1c02229>

## Notes

The authors declare no competing financial interest.

## ACKNOWLEDGMENTS

This project was supported by the Department of Energy Office of Basic Energy Sciences under Grant DE-SC0016390. A portion of this research used neutron research facilities at the Spallation Neutron Source, a DOE Office of Science User Facility operated by the Oak Ridge National Laboratory and the National Institute of Standards and Technology, U.S. Department of Commerce, supported in part by the National Science Foundation under Agreement DMR-1508 249. The MRL Shared Experimental Facilities are supported by the MRSEC Program of the NSF under Award DMR 1720 256, a member of the NSF-funded Materials Research Facilities Network. C.R.B. acknowledges support from the National Science and Engineering Research Council of Canada (NSERC) for a postdoctoral fellowship.

## REFERENCES

- (1) Jenekhe, S. A.; Osaheni, J. A. Excimers and Exciplexes of Conjugated Polymers. *Science* **1994**, *265*, 765–768.
- (2) Guo, X.; Baumgarten, M.; Mullen, K. Designing  $\pi$ -Conjugated Polymers for Organic Electronics. *Prog. Polym. Sci.* **2013**, *38*, 1832–1908.
- (3) Liu, C.; Wang, K.; Gong, X.; Heeger, A. J. Low Bandgap Semiconducting Polymers for Polymeric Photovoltaics. *Chem. Soc. Rev.* **2016**, *45*, 4848–4849.
- (4) Kim, M.; Ryu, S. U.; Park, S. A.; Choi, K.; Kim, T.; Chung, D.; Park, T. Donor-Acceptor-Conjugated Polymer for High-Performance Organic Field-Effect Transistors: A Progress Report. *Adv. Funct. Mater.* **2020**, *30*, 1904545.
- (5) Carbone, P.; Troisi, A. Charge Diffusion in Semiconducting Polymers: Analytical Relation between Polymer Rigidity and Time Scales for Intrachain and Interchain Hopping. *J. Phys. Chem. Lett.* **2014**, *5*, 2637–2641.
- (6) Gu, K. C.; Snyder, C. R.; Onorato, J.; Luscombe, C. K.; Bosse, A. W.; Loo, Y. L. Assessing the Huang-Brown Description of Tie Chains for Charge Transport in Conjugated Polymers. *ACS Macro Lett.* **2018**, *7*, 1333–1338.
- (7) Noriega, R.; Salleo, A.; Spakowitz, A. J. Chain Conformations Dictate Multiscale Charge Transport Phenomena in Disordered Semiconducting Polymers. *Proc. Natl. Acad. Sci. U. S. A.* **2013**, *110*, 16315–16320.
- (8) Zhang, X. R.; Bronstein, H.; Kronemeijer, A. J.; Smith, J.; Kim, Y.; Kline, R. J.; Richter, L. J.; Anthopoulos, T. D.; Sirringhaus, H.; Song, K.; Heeney, M.; Zhang, W. M.; McCulloch, I.; DeLongchamp, D. M. Molecular Origin of High Field-Effect Mobility in an Indacenodithiophene-Benzothiadiazole Copolymer. *Nat. Commun.* **2013**, *4*, 2238.
- (9) Venkateshvaran, D.; et al. Approaching Disorder-Free Transport in High-Mobility Conjugated Polymers. *Nature* **2014**, *515*, 384–388.
- (10) Prodhon, S.; Qiu, J.; Ricci, M.; Roscioni, O. M.; Wang, L. J.; Beljonne, D. Design Rules to Maximize Charge-Carrier Mobility along Conjugated Polymer Chains. *J. Phys. Chem. Lett.* **2020**, *11*, 6519–6525.
- (11) Fratini, S.; Nikolka, M.; Salleo, A.; Schweicher, G.; Sirringhaus, H. Charge Transport in High-Mobility Conjugated Polymers and Molecular Semiconductors. *Nat. Mater.* **2020**, *19*, 491–502.
- (12) Lemaur, V.; Cornil, J.; Lazzaroni, R.; Sirringhaus, H.; Beljonne, D.; Olivier, Y. Resilience to Conformational Fluctuations Controls Energetic Disorder in Conjugated Polymer Materials: Insights from Atomistic Simulations. *Chem. Mater.* **2019**, *31*, 6889–6899.
- (13) Wood, B. M.; Forse, A. C.; Persson, K. A. Aromaticity as a Guide to Planarity in Conjugated Molecules and Polymers. *J. Phys. Chem. C* **2020**, *124*, 5608–5612.
- (14) Gu, K. C.; Loo, Y. L. The Polymer Physics of Multiscale Charge Transport in Conjugated Systems. *J. Polym. Sci., Part B: Polym. Phys.* **2019**, *57*, 1559–1571.
- (15) Liu, C.; Hu, W.; Jiang, H.; Liu, G.; Han, C. C.; Sirringhaus, H.; Boué, F.; Wang, D. Chain Conformation and Aggregation Structure Formation of a High Charge Mobility DPP-Based Donor-Acceptor Conjugated Polymer. *Macromolecules* **2020**, *53*, 8255–8266.
- (16) Cohen, A. E.; Jackson, N. E.; de Pablo, J. J. Anisotropic Coarse-Grained Model for Conjugated Polymers: Investigations into Solution Morphologies. *Macromolecules* **2021**, *54*, 3780–3789.
- (17) Cendra, C.; Balhorn, L.; Zhang, W.; O'Hara, K.; Bruening, K.; Tassone, C. J.; Steinrück, H.-G.; Liang, M.; Toney, M. F.; McCulloch, I.; Chabinc, M. L.; Salleo, A.; Takacs, C. J. Unraveling the Unconventional Order of a High-Mobility Indacenodithiophene-Benzothiadiazole Copolymer. *ACS Macro Lett.* **2021**, *10*, 1306–1314.
- (18) Noriega, R.; Rivnay, J.; Vandewal, K.; Koch, F. P.; Stingelin, N.; Smith, P.; Toney, M. F.; Salleo, A. A General Relationship Between Disorder, Aggregation and Charge Transport in Conjugated Polymers. *Nat. Mater.* **2013**, *12*, 1038–44.
- (19) Chaudhry, S.; Wu, Y. K.; Cao, Z. Q.; Li, S.; Canada, J. L.; Gu, X. D.; Risko, C.; Mei, J. G. Evolution of Chain Dynamics and Oxidation States with Increasing Chain Length for a Donor-Acceptor-Conjugated Oligomer Series. *Macromolecules* **2021**, *54*, 8207–8219.
- (20) Zhang, W. L.; Gomez, E. D.; Milner, S. T. Predicting Chain Dimensions of Semiflexible Polymers from Dihedral Potentials. *Macromolecules* **2014**, *47*, 6453–6461.
- (21) McCulloch, B.; Ho, V.; Hoarfrost, M.; Stanley, C.; Do, C.; Heller, W. T.; Segalman, R. A. Polymer Chain Shape of Poly(3-alkylthiophenes) in Solution Using Small-Angle Neutron Scattering. *Macromolecules* **2013**, *46*, 1899–1907.
- (22) Kuei, B.; Gomez, E. D. Chain Conformations and Phase Behavior of Conjugated Polymers. *Soft Matter* **2017**, *13*, 49–67.
- (23) Danielsen, S. P. O.; Davidson, E. C.; Fredrickson, G. H.; Segalman, R. A. Absence of Electrostatic Rigidity in Conjugated Polyelectrolytes with Pendant Charges. *ACS Macro Lett.* **2019**, *8*, 1147–1152.
- (24) Aime, J. P.; Bargain, F. Comments on the Chain Conformation of Conjugated Polymers in Solution. *Europhys. Lett.* **1989**, *9*, 35–40.
- (25) Aime, J. P.; Bargain, F.; Schott, M.; Eckhardt, H.; Miller, G. G.; Elsenbaumer, R. L. Structural Study of Doped and Undoped Polythiophene in Solution by Small-Angle Neutron-Scattering. *Phys. Rev. Lett.* **1989**, *62*, 55–58.
- (26) Aime, J. P.; Garrin, P.; Baker, G. L.; Ramakrishnan, S.; Timmins, P. Physical Origin of the Local Rigidity of Conjugated Polymers in Good Solvent. *Synth. Met.* **1991**, *41*, 859–867.
- (27) Hong, W. D.; Lam, C. N.; Wang, Y. Y.; He, Y. J.; Sanchez-Diaz, L. E.; Do, C.; Chen, W. R. Influence of Side Chain Isomerism on the Rigidity of Poly(3-alkylthiophenes) in Solutions Revealed by Neutron Scattering. *Phys. Chem. Chem. Phys.* **2019**, *21*, 7745–7749.
- (28) Cao, Z.; Li, Z.; Zhang, S.; Galuska, L. A.; Li, T.; Do, C.; Xia, W.; Hong, K.; Gu, X. D. Decoupling Poly(3-alkylthiophenes)' Backbone and Side-Chain Conformation by Selective Deuteration and Neutron Scattering. *Macromolecules* **2020**, *53*, 11142–11152.
- (29) Fytas, G.; Nothofer, H. G.; Scherf, U.; Vlassopoulos, D.; Meier, G. Structure and Dynamics of Nondilute Polyfluorene Solutions. *Macromolecules* **2002**, *35*, 481–488.
- (30) Gettinger, C. L.; Heeger, A. J.; Drake, J. M.; Pine, D. J. A Photoluminescence Study of Poly(Phenylene Vinylene) Derivatives—the Effect of Intrinsic Persistence Length. *J. Chem. Phys.* **1994**, *101*, 1673–1678.
- (31) Gettinger, C. L.; Heeger, A. J.; Drake, J. M.; Pine, D. J. The Effect of Intrinsic Rigidity on the Optical-Properties of PPV Derivatives. *Mol. Cryst. Liq. Cryst. Sci. Technol., Sect. A* **1994**, *256*, 507–512.
- (32) Danielsen, S. P. O.; Sanoja, G. E.; McCuskey, S. R.; Hammouda, B.; Bazan, G. C.; Fredrickson, G. H.; Segalman, R. A. Mixed Conductive Soft Solids by Electrostatically Driven Network Formation of a Conjugated Polyelectrolyte. *Chem. Mater.* **2018**, *30*, 1417–1426.

- (33) Xi, Y. Y.; Wolf, C. M.; Pozzo, L. D. Self-Assembly of Donor-Acceptor Conjugated Polymers Induced by Miscible 'Poor' Solvents. *Soft Matter* **2019**, *15*, 1799–1812.
- (34) Reid, D. R.; Jackson, N. E.; Bourque, A. J.; Snyder, C. R.; Jones, R. L.; de Pablo, J. J. Aggregation and Solubility of a Model Conjugated Donor-Acceptor Polymer. *J. Phys. Chem. Lett.* **2018**, *9*, 4802–4807.
- (35) Bridges, C. R.; Ford, M. J.; Popere, B. C.; Bazan, G. C.; Segalman, R. A. Formation and Structure of Lyotropic Liquid Crystalline Mesophases in Donor-Acceptor Semiconducting Polymers. *Macromolecules* **2016**, *49*, 7220–7229.
- (36) Bridges, C. R.; Ford, M. J.; Bazan, G. C.; Segalman, R. A. Molecular Considerations for Mesophase Interaction and Alignment of Lyotropic Liquid Crystalline Semiconducting Polymers. *ACS Macro Lett.* **2017**, *6*, 619–624.
- (37) Bridges, C. R.; Ford, M. J.; Thomas, E. M.; Gomez, C.; Bazan, G. C.; Segalman, R. A. Effects of Side Chain Branch Point on Self Assembly, Structure, and Electronic Properties of High Mobility Semiconducting Polymers. *Macromolecules* **2018**, *51*, 8597–8604.
- (38) Jung, J. W.; Liu, F.; Russell, T. P.; Jo, W. H. Synthesis of Pyridine-Capped Diketopyrrolopyrrole and its Use as a Building Block of Low Band-Gap Polymers for Efficient Polymer Solar Cells. *Chem. Commun.* **2013**, *49*, 8495–8497.
- (39) Bridges, C. R.; Wang, M.; Ford, M. J.; Bazan, G. C.; Segalman, R. A. Branch Point Effect on Structure and Electronic Properties of Conjugated Polymers. US Patent Application No. 16/144,512. US Patent 20190181348, 2019.
- (40) Fair, R. A.; Xie, R. X.; Lee, Y.; Colby, R. H.; Gomez, E. D. Molecular Weight Characterization of Conjugated Polymers Through Gel Permeation Chromatography and Static Light Scattering. *ACS Appl. Polym. Mater.* **2021**, *3*, 4572–4578.
- (41) Higgins, J. S.; Benoit, H. C. *Polymers and Neutron Scattering*; Oxford University Press: New York, 1996.
- (42) Glinka, C. J.; Barker, J. G.; Hammouda, B.; Krueger, S.; Moyer, J. J.; Orts, W. J. The 30m Small-Angle Neutron Scattering Instruments at the National Institute of Standards and Technology. *J. Appl. Crystallogr.* **1998**, *31*, 430–445.
- (43) Zhao, J. K.; Gao, C. Y.; Liu, D. The Extended Q-Range Small-Angle Neutron Scattering Diffractometer at the SNS. *J. Appl. Crystallogr.* **2010**, *43*, 1068–1077.
- (44) Kline, S. R. Reduction and Analysis of SANS and USANS Data Using IGOR Pro. *J. Appl. Crystallogr.* **2006**, *39*, 895–900.
- (45) Wignall, G. D.; Bates, F. S. Absolute Calibration of Small-Angle Neutron-Scattering Data. *J. Appl. Crystallogr.* **1987**, *20*, 28–40.
- (46) Mantid: Manipulation and Analysis Toolkit for Instrument Data, 2013.
- (47) Arnold, O.; et al. Mantid—Data Analysis and Visualization Package for Neutron Scattering and  $\mu$ SR Experiments. *Nucl. Instrum. Methods Phys. Res., Sect. A* **2014**, *764*, 156–166.
- (48) Pedersen, J. S.; Schurtenberger, P. Scattering Functions of Semiflexible Polymers with and Without Excluded Volume Effects. *Macromolecules* **1996**, *29*, 7602–7612.
- (49) Chen, W. R.; Butler, P. D.; Magid, L. J. Incorporating Intermicellar Interactions in the Fitting of SANS Data from Cationic Worm-like Micelles. *Langmuir* **2006**, *22*, 6539–48.
- (50) Chai, J. D.; Head-Gordon, M. Systematic Optimization of Long-Range Corrected Hybrid Density Functionals. *J. Chem. Phys.* **2008**, *128*, 084106.
- (51) Darling, S. B.; Sternberg, M. Importance of Side Chains and Backbone Length in Defect Modeling of Poly(3-alkylthiophenes). *J. Phys. Chem. B* **2009**, *113*, 6215–6218.
- (52) Tsourtuou, F. D.; Peristeras, L. D.; Apostolov, R.; Mavrantzas, V. G. Molecular Dynamics Simulation of Amorphous Poly(3-hexylthiophene). *Macromolecules* **2020**, *53*, 7810–7824.
- (53) Dyson, M. J.; Lariou, E.; Martin, J.; Li, R. P.; Erothu, H.; Wantz, G.; Topham, P. D.; Dautel, O. J.; Hayes, S. C.; Stavrinou, P. N.; Stingelin, N. Managing Local Order in Conjugated Polymer Blends via Polarity Contrast. *Chem. Mater.* **2019**, *31*, 6540–6547.
- (54) Nagai, M.; Huang, J.; Zhou, T. D.; Huang, W. Effect of Molecular Weight on Conformational Characteristics of Poly(3-hexylthiophene). *J. Polym. Sci., Part B: Polym. Phys.* **2017**, *55*, 1273–1277.
- (55) Westenhoff, S.; Beenken, W. J. D.; Yartsev, A.; Greenham, N. C. Conformational Disorder of Conjugated Polymers. *J. Chem. Phys.* **2006**, *125*, 154903.
- (56) Brédas, J. L.; Street, G. B.; Themans, B.; Andre, J. M. Organic Polymers Based on Aromatic Rings (Polyparaphenylene, Polypyrrole, Polythiophene) - Evolution of the Electronic-Properties as a Function of the Torsion Angle between Adjacent Rings. *J. Chem. Phys.* **1985**, *83*, 1323–1329.
- (57) McCulloch, I.; Ashraf, R. S.; Biniek, L.; Bronstein, H.; Combe, C.; Donaghey, J. E.; James, D. I.; Nielsen, C. B.; Schroeder, B. C.; Zhang, W. M. Design of Semiconducting Indacenodithiophene Polymers for High Performance Transistors and Solar Cells. *Acc. Chem. Res.* **2012**, *45*, 714–722.
- (58) Wadsworth, A.; Chen, H.; Thorley, K. J.; Cendra, C.; Nikolka, M.; Bristow, H.; Moser, M.; Salleo, A.; Anthopoulos, T. D.; Sirringhaus, H.; McCulloch, I. Modification of Indacenodithiophene-Based Polymers and Its Impact on Charge Carrier Mobility in Organic Thin-Film Transistors. *J. Am. Chem. Soc.* **2020**, *142*, 652–664.
- (59) Jackson, N. E.; Savoie, B. M.; Kohlstedt, K. L.; Olvera de la Cruz, M.; Schatz, G. C.; Chen, L. X.; Ratner, M. A. Controlling Conformations of Conjugated Polymers and Small Molecules: The Role of Nonbonding Interactions. *J. Am. Chem. Soc.* **2013**, *135*, 10475–10483.
- (60) Wang, Q.; Böckmann, S.; Günther, F.; Streiter, M.; Zerson, M.; Scaccabarozzi, A. D.; Tan, W. L.; Komber, H.; Deibel, C.; Magerle, R.; Gemming, S.; McNeill, C. R.; Caironi, M.; Hansen, M. R.; Sommer, M. Hydrogen Bonds Control Single-Chain Conformation, Crystallinity, and Electron Transport in Isoelectronic Diketopyrrolopyrrole Copolymers. *Chem. Mater.* **2021**, *33*, 2635–2645.
- (61) Liu, X. F.; Sun, Y. M.; Hsu, B. B. Y.; Lorbach, A.; Qi, L.; Heeger, A. J.; Bazan, G. C. Design and Properties of Intermediate-Sized Narrow Band-Gap Conjugated Molecules Relevant to Solution-Processed Organic Solar Cells. *J. Am. Chem. Soc.* **2014**, *136*, 5697–5708.
- (62) Karunasena, C.; Li, S.; Heifner, M. C.; Ryno, S. M.; Risko, C. Reconsidering the Roles of Noncovalent Intramolecular "Locks" in  $\pi$ -Conjugated Molecules. *Chem. Mater.* **2021**, *33*, 9139–9151.
- (63) Bombile, J. H.; Janik, M. J.; Milner, S. T. Tight Binding Model of Conformational Disorder Effects on the Optical Absorption Spectrum of Polythiophenes. *Phys. Chem. Chem. Phys.* **2016**, *18*, 12521–12533.
- (64) Bombile, J. H.; Janik, M. J.; Milner, S. T. Polaron Formation Mechanisms in Conjugated Polymers. *Phys. Chem. Chem. Phys.* **2018**, *20*, 317–331.
- (65) Sun, B.; Hong, W.; Yan, Z. Q.; Aziz, H.; Li, Y. N. Record High Electron Mobility of  $6.3 \text{ cm}^2\text{V}^{-1}\text{s}^{-1}$  Achieved for Polymer Semiconductors Using a New Building Block. *Adv. Mater.* **2014**, *26*, 2636–2642.
- (66) Wang, Z.-Y.; Yao, Z.-F.; Lu, Y.; Ding, L.; Yu, Z.-D.; You, H.-Y.; Wang, X.-Y.; Zhou, Y.-Y.; Zou, L.; Wang, J.-Y.; Pei, J. Precise Tracking and Modulating Aggregation Structures of Conjugated Copolymers in Solutions. *Polym. Chem.* **2020**, *11*, 3716–3722.
- (67) Dixon, A. G.; Visvanathan, R.; Clark, N. A.; Stingelin, N.; Kopidakis, N.; Shaheen, S. E. Molecular Weight Dependence of Carrier Mobility and Recombination Rate in Neat P3HT Films. *J. Polym. Sci., Part B: Polym. Phys.* **2018**, *56*, 31–35.
- (68) Mollinger, S. A.; Krajina, B. A.; Noriega, R.; Salleo, A.; Spakowitz, A. J. Percolation, Tie-Molecules, and the Microstructural Determinants of Charge Transport in Semicrystalline Conjugated Polymers. *ACS Macro Lett.* **2015**, *4*, 708–712.
- (69) Thomas, T. H.; Harkin, D. J.; Gillett, A. J.; Lemaire, V.; Nikolka, M.; Sadhanala, A.; Richter, J. M.; Armitage, J.; Chen, H.; McCulloch, I.; Menke, S. M.; Olivier, Y.; Beljonne, D.; Sirringhaus, H. Short Contacts Between Chains Enhancing Luminescence Quantum Yields

and Carrier Mobilities in Conjugated Copolymers. *Nat. Commun.* **2019**, *10*, 2614.

(70) Chen, H.; et al. The Effect of Ring Expansion in Thienobenzobenzene Polymers for Organic Field-Effect Transistors. *J. Am. Chem. Soc.* **2019**, *141*, 18806–18813.

(71) Cao, Z. Q.; Leng, M. W.; Cao, Y. R.; Gu, X. D.; Fang, L. How Rigid Are Conjugated Non-Ladder and Ladder Polymers? *J. Polym. Sci.* **2021**, *59*, 1–13.

(72) Raithel, D.; Simine, L.; Pickel, S.; Schotz, K.; Panzer, F.; Baderschneider, S.; Schiefer, D.; Lohwasser, R.; Kohler, J.; Thelakkat, M.; Sommer, M.; Kohler, A.; Rossky, P. J.; Hildner, R. Direct Observation of Backbone Planarization via Side-Chain Alignment in Single Bulky-Substituted Polythiophenes. *Proc. Natl. Acad. Sci. U. S. A.* **2018**, *115*, 2699–2704.

(73) Chew, A. R.; Ghosh, R.; Pakhnyuk, V.; Onorato, J.; Davidson, E. C.; Segalman, R. A.; Luscombe, C. K.; Spano, F. C.; Salleo, A. Unraveling the Effect of Conformational and Electronic Disorder in the Charge Transport Processes of Semiconducting Polymers. *Adv. Funct. Mater.* **2018**, *28*, 1804142.

(74) Barford, W.; Marcus, M. Perspective: Optical Spectroscopy in  $\pi$ -Conjugated Polymers and How It Can Be Used To Determine Multiscale Polymer Structures. *J. Chem. Phys.* **2017**, *146*, 130902.

(75) Panzer, F.; Bassler, H.; Kohler, A. Temperature Induced Order-Disorder Transition in Solutions of Conjugated Polymers Probed by Optical Spectroscopy. *J. Phys. Chem. Lett.* **2017**, *8*, 114–125.

(76) Wedler, S.; Zhou, C.; Bazan, G. C.; Panzer, F.; Köhler, A. Role of Torsional Flexibility in the Film Formation Process in Two  $\pi$ -Conjugated Model Oligomers. *J. Phys. Chem. Lett.* **2020**, *11*, 9379–9386.

(77) Wedler, S.; Bourdick, A.; Athanasopoulos, S.; Gekle, S.; Panzer, F.; McDowell, C.; Nguyen, T. Q.; Bazan, G. C.; Köhler, A. What is the Role of Planarity and Torsional Freedom for Aggregation in a  $\pi$ -Conjugated Donor-Acceptor Model Oligomer? *J. Mater. Chem. C* **2020**, *8*, 4944–4955.

(78) McDearmon, B.; Lim, E.; Lee, I. H.; Kozycz, L. M.; O'Hara, K.; Robledo, P. I.; Venkatesan, N. R.; Chabiny, M. L.; Hawker, C. J. Effects of Side-Chain Topology on Aggregation of Conjugated Polymers. *Macromolecules* **2018**, *51*, 2580–2590.

(79) Sugiyama, F.; Kleinschmidt, A. T.; Kayser, L. V.; Rodriguez, D.; Finn, M.; Alkhadra, M. A.; Wan, J. M. H.; Ramirez, J.; Chiang, A. S. C.; Root, S. E.; Savagatrup, S.; Lipomi, D. J. Effects of Flexibility and Branching of Side Chains on the Mechanical Properties of Low-Bandgap Conjugated Polymers. *Polym. Chem.* **2018**, *9*, 4354–4363.

(80) Cao, Z. Q.; Galuska, L.; Qian, Z. Y.; Zhang, S.; Huang, L. F.; Prine, N.; Li, T. Y.; He, Y. J.; Hong, K. L.; Gu, X. D. The Effect of Side-Chain Branch Position on the Thermal Properties of Poly(3-alkylthiophenes). *Polym. Chem.* **2020**, *11*, 517–526.

(81) Zhan, P. F.; Zhang, W. L.; Jacobs, I. E.; Nisson, D. M.; Xie, R. X.; Weissen, A. R.; Colby, R. H.; Moule, A. J.; Milner, S. T.; Maranas, J. K.; Gomez, E. D. Side Chain Length Affects Backbone Dynamics in Poly(3-Alkylthiophene)s. *J. Polym. Sci., Part B: Polym. Phys.* **2018**, *56*, 1193–1202.

(82) Adachi, T.; Brazard, J.; Ono, R. J.; Hanson, B.; Traub, M. C.; Wu, Z.-Q.; Li, Z.; Bolinger, J. C.; Ganesan, V.; Bielawski, C. W.; Vanden Bout, D. A.; Barbara, P. F. Regioregularity and Single Polythiophene Chain Conformation. *J. Phys. Chem. Lett.* **2011**, *2*, 1400–1404.

(83) Chen, A. X.; Kleinschmidt, A. T.; Choudhary, K.; Lipomi, D. J. Beyond Stretchability: Strength, Toughness, and Elastic Range in Semiconducting Polymers. *Chem. Mater.* **2020**, *32*, 7582–7601.

(84) Tegegne, N. A.; Abdissa, Z.; Mammo, W.; Uchiyama, T.; Okada-Shudo, Y.; Galeotti, F.; Porzio, W.; Andersson, M. R.; Schlettwein, D.; Vohra, V.; Schwoerer, H. Effect of Alkyl Side Chain Length on Intra- and Intermolecular Interactions of Terthiophene-Isoindigo Copolymers. *J. Phys. Chem. C* **2020**, *124*, 9644–9655.

(85) Himmelberger, S.; Duong, D. T.; Northrup, J. E.; Rivnay, J.; Koch, F. P. V.; Beckingham, B. S.; Stingelin, N.; Segalman, R. A.; Mannsfeld, S. C. B.; Salleo, A. Role of Side-Chain Branching on Thin-

Film Structure and Electronic Properties of Polythiophenes. *Adv. Funct. Mater.* **2015**, *25*, 2616–2624.

(86) Meyer, D. L.; Schmidt-Meinzer, N.; Matt, C.; Rein, S.; Lombeck, F.; Sommer, M.; Biskup, T. Side-Chain Engineering of Conjugated Polymers: Distinguishing Its Impact on Film Morphology and Electronic Structure. *J. Phys. Chem. C* **2019**, *123*, 20071–20083.

(87) Fu, B. Y.; Baltazar, J.; Sankar, A. R.; Chu, P. H.; Zhang, S. Y.; Collard, D. M.; Reichmanis, E. Enhancing Field-Effect Mobility of Conjugated Polymers Through Rational Design of Branched Side Chains. *Adv. Funct. Mater.* **2014**, *24*, 3734–3744.

(88) Li, Z.; Tsang, S. W.; Du, X. M.; Scoles, L.; Robertson, G.; Zhang, Y. G.; Toll, F.; Tao, Y.; Lu, J. P.; Ding, J. F. Alternating Copolymers of Cyclopenta[2,1-b;3,4-b']dithiophene and Thieno[3,4-c]pyrrole-4,6-dione for High-Performance Polymer Solar Cells. *Adv. Funct. Mater.* **2011**, *21*, 3331–3336.

(89) Moser, M.; Savagian, L. R.; Savva, A.; Matta, M.; Ponder, J. F.; Hidalgo, T. C.; Ohayon, D.; Hallani, R.; Reijjalali, M.; Troisi, A.; Wadsworth, A.; Reynolds, J. R.; Inal, S.; McCulloch, I. Ethylene Glycol-Based Side Chain Length Engineering in Polythiophenes and its Impact on Organic Electrochemical Transistor Performance. *Chem. Mater.* **2020**, *32*, 6618–6628.

(90) Themans, B.; Salaneck, W. R.; Brédas, J. L. Theoretical-Study of the Influence of Thermochemical Effects on the Electronic-Structure of Poly(3-Hexylthiophene). *Synth. Met.* **1989**, *28*, C359–C364.

(91) Hu, Z. J.; Adachi, T.; Lee, Y. G.; Haws, R. T.; Hanson, B.; Ono, R. J.; Bielawski, C. W.; Ganesan, V.; Rossky, P. J.; Vanden Bout, D. A. Effect of the Side-Chain-Distribution Density on the Single-Conjugated-Polymer-Chain Conformation. *ChemPhysChem* **2013**, *14*, 4143–4148.

(92) Yang, Y. Z.; Liu, Z. T.; Zhang, G. X.; Zhang, X. S.; Zhang, D. Q. The Effects of Side Chains on the Charge Mobilities and Functionalities of Semiconducting Conjugated Polymers beyond Solubilities. *Adv. Mater.* **2019**, *31*, 1903104.

(93) Lei, T.; Dou, J. H.; Pei, J. Influence of Alkyl Chain Branching Positions on the Hole Mobilities of Polymer Thin-Film Transistors. *Adv. Mater.* **2012**, *24*, 6457–6461.

(94) Kang, I.; Yun, H. J.; Chung, D. S.; Kwon, S. K.; Kim, Y. H. Record High Hole Mobility in Polymer Semiconductors via Side-Chain Engineering. *J. Am. Chem. Soc.* **2013**, *135*, 14896–14899.

(95) Mei, J. G.; Bao, Z. N. Side Chain Engineering in Solution-Processable Conjugated Polymers. *Chem. Mater.* **2014**, *26*, 604–615.

(96) Thomas, T. H.; Rivett, J. P. H.; Gu, Q. F.; Harkin, D. J.; Richter, J. M.; Sadhanala, A.; Yong, C. K.; Schott, S.; Broch, K.; Armitage, J.; Gillett, A. J.; Menke, S. M.; Rao, A.; Credgington, D.; Siringhaus, H. Chain Coupling and Luminescence in High-Mobility, Low-Disorder Conjugated Polymers. *ACS Nano* **2019**, *13*, 13716–13727.

(97) Ochieng, M. A.; Ponder, J. F.; Reynolds, J. R. Effects of Linear and Branched Side Chains on the Redox and Optoelectronic Properties of 3,4-dialkoxythiophene Polymers. *Polym. Chem.* **2020**, *11*, 2173–2181.

(98) Kerszulis, J. A.; Johnson, K. E.; Kuepfert, M.; Khoshabo, D.; Dyer, A. L.; Reynolds, J. R. Tuning the Painter's Palette: Subtle Steric Effects on Spectra and Colour in Conjugated Electrochromic Polymers. *J. Mater. Chem. C* **2015**, *3*, 3211–3218.

(99) McDearmon, B.; Page, Z. A.; Chabiny, M. L.; Hawker, C. J. Organic Electronics by Design: the Power of Minor Atomic and Structural changes. *J. Mater. Chem. C* **2018**, *6*, 3564–3572.

(100) Nguyen, T.-Q.; Doan, V.; Schwartz, B. J. Conjugated Polymer Aggregates in Solution: Control of Interchain Interactions. *J. Chem. Phys.* **1999**, *110*, 4068–4078.

(101) Hua, C. C.; Kuo, C. Y.; Chen, S. A. Controlling Bulk Aggregation State in Semiconducting Conjugated Polymer Solution. *Appl. Phys. Lett.* **2008**, *93*, 123303.

(102) Vogelsang, J.; Adachi, T.; Brazard, J.; Vanden Bout, D. A.; Barbara, P. F. Self-Assembly of Highly Ordered Conjugated Polymer Aggregates with Long-Range Energy Transfer. *Nat. Mater.* **2011**, *10*, 942–946.

(103) Schaefer, D. W.; Joanny, J. F.; Pincus, P. Dynamics of Semiflexible Polymers in Solution. *Macromolecules* **1980**, *13*, 1280–1289.

(104) Moon, J.; Nakanishi, H. Onset of the Excluded-Volume Effect for the Statistics of Stiff Chains. *Phys. Rev. A* **1991**, *44*, 6427–6442.

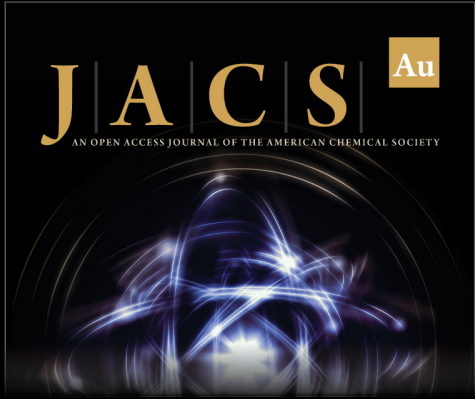
(105) Newbloom, G. M.; Weigandt, K. M.; Pozzo, L. D. Electrical, Mechanical, and Structural Characterization of Self-Assembly in Poly(3-hexylthiophene) Organogel Networks. *Macromolecules* **2012**, *45*, 3452–3462.

(106) Newbloom, G. M.; Weigandt, K. M.; Pozzo, L. D. Structure and Property Development of Poly(3-hexylthiophene) Organogels Probed with Combined Rheology, Conductivity and Small Angle Neutron Scattering. *Soft Matter* **2012**, *8*, 8854–8864.

(107) Newbloom, G. M.; Kim, F. S.; Jenekhe, S. A.; Pozzo, L. D. Mesoscale Morphology and Charge Transport in Colloidal Networks of Poly(3-hexylthiophene). *Macromolecules* **2011**, *44*, 3801–3809.

(108) Knaapila, M.; Monkman, A. P. Methods for Controlling Structure and Photophysical Properties in Polyfluorene Solutions and Gels. *Adv. Mater.* **2013**, *25*, 1090–108.

(109) Knaapila, M.; Stewart, B.; Garamus, V. M.; Ramos, M. L.; Cruz, P. F.; Brito, R. M. M.; Justino, L. L. G.; Fausto, R.; Napierala, C.; Forster, M.; Burrows, H. D.; Scherf, U. Poly(9-undecyl-9-methyl-fluorene) and Poly(9-pentadecyl-9-methyl-fluorene): Synthesis, Solution Structure, and Effect of Side Chain Asymmetry on Aggregation Behavior. *J. Polym. Sci., Part B: Polym. Phys.* **2019**, *57*, 826–837.



**JACS Au**  
AN OPEN ACCESS JOURNAL OF THE AMERICAN CHEMICAL SOCIETY

 Editor-in-Chief  
**Prof. Christopher W. Jones**  
Georgia Institute of Technology, USA

**Open for Submissions** 

pubs.acs.org/jacsau  ACS Publications  
Most Trusted. Most Cited. Most Read.